

An analytical model for the slip velocity of particles in turbulence

Tim Berk^{1,†} and Filippo Coletti²

¹Department of Mechanical and Aerospace Engineering, Utah State University, Logan, UT 84322, USA

²Department of Mechanical and Process Engineering, ETH Zurich, 8092 Zurich, Switzerland

(Received 12 April 2024; revised 18 June 2024; accepted 21 June 2024)

Predicting the magnitude of the slip velocity of non-tracer particles with respect to the surrounding fluid is crucial to address both fundamental and practical questions involving dispersed turbulent flows. Here we derive an analytical model to predict the slip velocity of spherical particles in homogeneous isotropic turbulence. We modulate the particle equation of motion according to the inertial filtering framework, and obtain closed-form expressions for the mean slip velocity magnitude as a function of the governing parameters. These are compared against laboratory measurements and direct numerical simulations, demonstrating close agreement for both light and heavy particles, both smaller and larger than the Kolmogorov scales. The predictive value of the model and its implications are discussed, as well as the range of validity of the underlying assumptions.

Key words: multiphase and particle-laden flows, turbulent flows

1. Introduction

Predicting the motion of small particles in a turbulent flow stands among the most fundamental questions in fluid dynamics. The instances in which the problem is relevant are uncountable, from atmospheric precipitation to pollutant dispersion, from chemical reactors to dust storms, from marine litter to planetesimal formation. The class of particles that can be considered as tracers, i.e. behaving as fluid parcels, is very limited: their size and response time must be small compared with the characteristic spatial and temporal scales of the flow, respectively; their density must approximate the one of the carrier phase; and their dilution must be sufficient to prevent collective effects (Brandt & Coletti 2022). In all other situations, the particle trajectories are expected to depart from fluid

† Email address for correspondence: tim.berk@usu.edu

pathlines, as quantified by the slip velocity $\mathbf{u}_s = \mathbf{u} - \mathbf{v}$ between the particle velocity \mathbf{v} and the fluid velocity at the particle location \mathbf{u} . This quantity profoundly impacts the spatial distribution, spreading rate, collision probability and gravitational drift of the dispersed phase (Balachandar & Eaton 2010; Pumir & Wilkinson 2016; Mathai, Lohse & Sun 2020; Bec, Gustavsson & Mehlig 2024). Moreover, \mathbf{u}_s contributes to defining the flow regime around the particles, features in the formulation of surface forces exerted on them by the fluid and is key for turbulence modification (Bellani & Variano 2012; Ling, Parmar & Balachandar 2013; Maxey 2017; Oka & Goto 2022; Balachandar, Peng & Wang 2024). In the context of numerical simulations, \mathbf{u}_s is also a primary parameter to select the appropriate computational approach (Balachandar 2009; Tenneti & Subramaniam 2014). It is therefore highly desirable to accurately estimate the slip velocity *a priori* from the governing parameters. Only scaling arguments are available (see, e.g., Balachandar 2009) which, while insightful, can only provide order-of-magnitude estimates.

Here we present an analytical model to predict the mean slip velocity magnitude of spherical particles in homogeneous isotropic turbulence. This is built on the framework of inertial filtering and rooted in the classic work of Csanady (1963) which we recently extended in Berk & Coletti (2021). In § 2, we obtain closed-form expressions of the slip velocity based on the non-dimensional governing parameters. In § 3, we demonstrate agreement with experiments and direct numerical simulations over a vast range of particle properties and flow regimes. We draw conclusions and provide an outlook in § 4.

2. Definitions and model derivation

We consider spherical particles of diameter d_p and density ρ_p in a fluid of density ρ_f and kinematic viscosity ν . The flow follows the canons of homogeneous isotropic turbulence, with Kolmogorov length, time and velocity scales η , τ_η and u_η , respectively, the corresponding integral scales being L , T and U . The Reynolds numbers characterising the flow around the particle and the turbulence are $Re_p = \langle |\mathbf{u}_s| \rangle d_p / \nu$ and $Re_\lambda = U\lambda / \nu$, respectively, where λ is the Taylor microscale. Here and in the following, angle brackets indicate statistical averaging.

The force balance on each particle is expressed according to (Gatignol 1983; Maxey & Riley 1983):

$$\rho_p \frac{\pi d_p^3}{6} \frac{d\mathbf{v}}{dt} = \mathbf{F}_d + \mathbf{F}_g + \mathbf{F}_b + \mathbf{F}_{am} + \mathbf{F}_{sg}, \quad (2.1)$$

where the right-hand side includes drag, gravity, buoyancy, added mass and stress gradient forces, respectively. They are expressed as

$$\mathbf{F}_d = 3\pi\rho_f\nu d_p \mathbf{u}_s \phi(Re_p), \quad (2.2a)$$

$$\mathbf{F}_g = -\frac{\pi d_p^3}{6} \rho_p \mathbf{g}, \quad (2.2b)$$

$$\mathbf{F}_b = \frac{\pi d_p^3}{6} \rho_f \mathbf{g}, \quad (2.2c)$$

$$\mathbf{F}_{am} = \frac{\pi d_p^3}{6} \rho_f C_M \left(\frac{D\mathbf{u}}{Dt} - \frac{d\mathbf{v}}{dt} \right), \quad (2.2d)$$

$$\mathbf{F}_{sg} = \frac{\pi d_p^3}{6} \rho_f \frac{D\mathbf{u}}{Dt}, \quad (2.2e)$$

where \mathbf{g} is the gravitational acceleration, C_M is the added mass coefficient, $\phi(Re_p)$ incorporates finite- Re_p effects in the Stokes' drag coefficient, $C_D = (24/Re_p)\phi(Re_p)$. We use the Schiller and Naumann expression $\phi(Re_p) = 1 + 0.15Re_p^{0.687}$ (Clift, Grace & Weber 2005).

In (2.1) we have omitted the history force, whose formulation presents well-known theoretical and numerical difficulties (Haller 2019). While effective strategies for its evaluation have been proposed recently (Parmar *et al.* 2018; Prasath, Vasan & Govindarajan 2019), the implementation in actual turbulent flows is still under development. Its omission here does not imply the effect being negligible (as its significance has been demonstrated in several situations (Olivieri *et al.* 2014; Daitche 2015)), but rather reflects the lack of a simple scaling for it. The lift force is also omitted, which is strictly reasonable only if $Re_p \ll 1$ or if the particle rotation is negligible (Saffman 1956; Rubinow & Keller 1961). The comparison of the proposed model against numerical and experimental data will confirm that such omissions are acceptable for the specific purpose of estimating the magnitude of the slip velocity. This stand is revisited in § 4.

The particle response time is defined as $\tau_p = d_p^2(1 + C_M)/(18\nu\beta\phi(Re_p))$, where $\beta = (1 + C_M)/(\rho + C_M)$ and $\rho = \rho_p/\rho_f$ is the density ratio. For spherical particles, $C_M = 1/2$, such that $\beta = 3/(2\rho + 1)$ and $\tau_p = d_p^2/(12\nu\beta\phi(Re_p))$. The Stokes number $St = \tau_p/\tau_\eta$ and the Froude number $Fr = a_\eta/(g|(1 - \beta)|)$, where $a_\eta = u_\eta/\tau_\eta$, express the importance of inertia and gravity for the particle motion, respectively.

We aim to estimate the statistical average of the slip velocity magnitude, which we approximate as $\langle |u_s| \rangle \approx (\langle |u_{s,1}| \rangle^2 + \langle |u_{s,2}| \rangle^2 + \langle |u_{s,3}| \rangle^2)^{1/2}$. All velocities in the following derivation are vector components $u_{s,i}$, but for brevity we omit the subscript i . To expand $\langle |u_s| \rangle$, we assume a Gaussian probability distribution $f(u_s)$ for each component. This is consistent with observations of heavy particles in homogeneous turbulence; see, e.g., measurements by Berk & Coletti (2021) shown in figure 1(a). The intermittency (observed especially for $St \gg 1$) may be incorporated in different forms of $f(u_s)$, though this will be shown to be unnecessary for the present purposes. Integration of $f(u_s)$ leads to

$$\langle |u_s| \rangle = |u_s| \operatorname{erf} \left\{ \left(\frac{1}{2} \frac{\langle u_s \rangle^2}{\langle u_s'^2 \rangle} \right)^{1/2} \right\} + \left(\frac{2}{\pi} \right)^{1/2} \langle u_s'^2 \rangle^{1/2} \exp \left\{ -\frac{1}{2} \frac{\langle u_s \rangle^2}{\langle u_s'^2 \rangle} \right\}, \quad (2.3)$$

where the prime denotes fluctuations around the mean. The mean slip velocity $\langle u_s \rangle$ is typically caused by gravity (or other body forces), whereas the variance of the slip velocity $\langle u_s'^2 \rangle$ is a result of turbulent fluctuations. As such, the ratio $\langle u_s \rangle / \langle u_s'^2 \rangle^{1/2}$ discriminates between turbulence-dominated and gravity-dominated regimes, with the transition around $\langle u_s \rangle / \langle u_s'^2 \rangle^{1/2} \approx 1$. This is illustrated in figure 1(b), where $\langle |u_s| \rangle / \langle u_s \rangle$ is modelled according to (2.3) and exhibits the scaling $\langle |u_s| \rangle \propto \langle u_s'^2 \rangle^{1/2}$ and $\langle |u_s| \rangle = \langle u_s \rangle$ in the respective regimes.

2.1. Heavy particles ($\rho \gg 1$)

The model takes two different forms in the limits $\rho \gg 1$ and $\rho \ll 1$. In the former case, the unsteady forces F_{am} and F_{sg} are at most of order $O(F_d St / (\rho - 1))$ (Ling *et al.* 2013). As such they are expected to be negligible in this limit, and the equation of motion simplifies

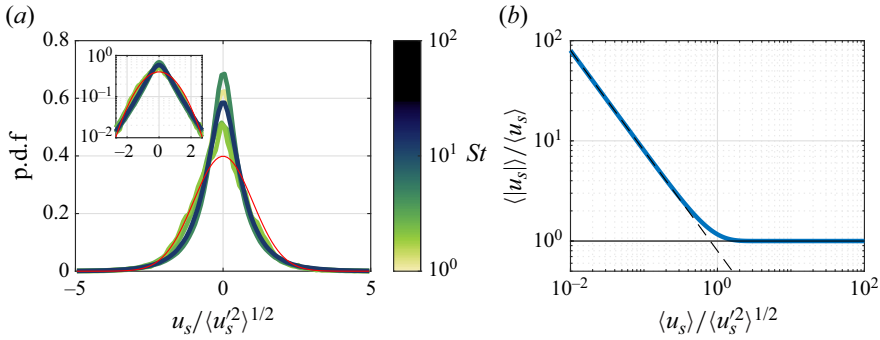


Figure 1. (a) Distribution of horizontal slip velocity component for various cases of heavy particles in turbulence, compared with a Gaussian distribution as indicated by the red line; inset shows a semi-log comparison. (b) Result from (2.3), illustrating switching behaviour between the turbulence-driven regime $\langle |u_s| \rangle \propto \langle u_s'^2 \rangle^{1/2}$ indicated by the dashed line and the settling-driven regime $\langle |u_s| \rangle = \langle u_s \rangle$ indicated by the solid line.

to

$$\frac{dv}{dt} = \frac{u_s}{\tau_p} - g(1 - 1/\rho). \tag{2.4}$$

The mean and variance of the slip velocity are, respectively,

$$\langle u_s \rangle = \tau_p g(1 - 1/\rho), \tag{2.5}$$

$$\langle u_s'^2 \rangle = \tau_p^2 \left\langle \left(\frac{dv'}{dt} \right)^2 \right\rangle, \tag{2.6}$$

where we have assumed steady state. The particle acceleration variance can be expressed as the integral of the acceleration spectrum $\omega^2 E_p(\omega)$ (Sawford 1991), where E_p represents the energy spectrum and ω is the Lagrangian angular frequency:

$$\left\langle \left(\frac{dv'}{dt} \right)^2 \right\rangle = \frac{2}{\pi} \int_0^\infty \omega^2 E_p(\omega) d\omega. \tag{2.7}$$

The acceleration spectrum of the particle is modelled using the inertial filtering framework proposed by Csanady (1963) and extended in Berk & Coletti (2021). In particular, a response function links the spectrum associated to the particle fluctuating energy, E_p , to the spectrum of the fluctuating energy of the fluid at the particle location, E :

$$E_p(\omega) = H^2(\omega)E(\omega). \tag{2.8}$$

This response function can be derived by Fourier-transform of the particle and fluid velocities, and for heavy particles we take (Csanady 1963)

$$H^2(\omega) = \frac{1}{1 + (\omega\tau_p)^2}. \tag{2.9}$$

The energy spectrum of the flow, in turn, is the Fourier transform of the velocity autocorrelation $R(\tau)$. Various expressions exist for the latter; here we use the two-timescale model proposed by Sawford (1991) with a short timescale T_2 , which leads to a horizontal

Model for the slip velocity of particles in turbulence

asymptote $R(\tau = 0)$ and curvature proportional to the acceleration variance (Mordant, L ev eque & Pinton 2004):

$$R(\tau) = \langle u'^2 \rangle \frac{T_L \exp(-\tau/T_L) - T_2 \exp(-\tau/T_2)}{T_L - T_2}. \quad (2.10)$$

Here T_L is the Lagrangian timescale of the flow observed by the particles. The two-timescale model has the benefit of yielding a finite-valued integral in (2.7), which is not the case when modelling the velocity autocorrelation using the integral timescale only (Zhang, Legendre & Zamansky 2019). This leads to

$$E(\omega) = \langle u'^2 \rangle \frac{T_L + T_2}{(1 + (\omega T_L)^2)(1 + (\omega T_2)^2)}. \quad (2.11)$$

Using (2.7)–(2.11), the slip velocity variance in (2.6) is given by

$$\langle u_s'^2 \rangle = \langle u'^2 \rangle \frac{\tau_p^2}{(T_L + \tau_p)(T_2 + \tau_p)}. \quad (2.12)$$

The mean slip velocity can then be expressed substituting (2.5) and (2.12) into (2.3). Upon normalisation by Kolmogorov units and substituting St and Fr , we have

$$\frac{\langle |u_s| \rangle}{u_\eta} = St Fr^{-1} \operatorname{erf} \left\{ \left(\frac{1}{2} \frac{\langle u_s \rangle^2}{\langle u_s'^2 \rangle} \right)^{1/2} \right\} + St \left(\frac{2}{\pi} \frac{\langle u'^2 \rangle}{u_\eta^2} \frac{1}{(T_L/\tau_\eta + St)(T_2/\tau_\eta + St)} \right)^{1/2} \exp \left\{ -\frac{1}{2} \frac{\langle u_s \rangle^2}{\langle u_s'^2 \rangle} \right\}, \quad (2.13)$$

with

$$\frac{\langle u_s \rangle^2}{\langle u_s'^2 \rangle} = \frac{u_\eta^2}{\langle u'^2 \rangle} Fr^{-2} (T_L/\tau_\eta + St)(T_2/\tau_\eta + St). \quad (2.14)$$

The time and velocity scales T_L , T_2 and $\langle u'^2 \rangle$ represent quantities observed by the particles. These potentially differ from scales observed by tracers, and in Berk & Coletti (2021) we evaluated them by applying corrections to the unconditional scales (Csanady 1963; Sawford 1991; Pozorski & Minier 1998). Here we use uncorrected scales, which simplifies the analysis and is expected to result in negligible quantitative differences (as shown in Berk & Coletti (2021) and confirmed in the following validation). The timescale and velocity ratios in (2.13) and (2.14) can be expressed as functions of Re_λ , using established relations for homogeneous isotropic turbulence: $\langle u'^2 \rangle / u_\eta^2 = Re_\lambda / 15^{1/2}$ (Hinze 1975), $T_L / \tau_\eta = 2(Re_\lambda + 32) / (15^{1/2} C_0)$ (Zaichik, Simonin & Alipchenkov 2003) and $T_2 / \tau_\eta = C_0 / (2a_0)$ (Sawford 1991) where $a_0 = 5 / (1 + 110 / Re_\lambda)$ (Sawford *et al.* 2003), $C_0 = C_0^\infty (1 - (0.1 Re_\lambda)^{-1/2})$ for $Re_\lambda > 50$ or $C_0 = 0.07 C_0^\infty Re_\lambda^{1/2}$ for $Re_\lambda < 50$ (Lien & D'Asaro 2002) and $C_0^\infty \approx 6 \pm 0.5$ (Ouellette *et al.* 2006). The lengthy final expression of $\langle |u_s| \rangle / u_\eta$, reported in Appendix A, represents a closed form of the mean slip velocity as a function of the governing parameters St , Fr and Re_λ .

2.2. Light particles ($\rho \ll 1$)

For particles much lighter than the fluid, the unsteady forces shall be retained and the equation of motion reads

$$\frac{dv}{dt} = \frac{u_s}{\tau_p} + \beta \frac{Du}{Dt} - g(1 - \beta). \tag{2.15}$$

From (2.15), the mean and variance of the slip velocity are, respectively,

$$\langle u_s \rangle = \tau_p g(1 - \beta), \tag{2.16}$$

$$\langle u_s'^2 \rangle = \tau_p^2 \left\langle \left(\frac{dv'}{dt} \right)^2 \right\rangle + \tau_p^2 \beta^2 \left\langle \left(\frac{Du'}{Dt} \right)^2 \right\rangle - 2\tau_p^2 \beta \left\langle \frac{dv'}{dt} \frac{Du'}{Dt} \right\rangle. \tag{2.17}$$

The variance of the particle acceleration is again modelled using the inertial filtering framework, albeit with a modified response function valid for light particles (Zhang *et al.* 2019):

$$H^2(\omega) = \frac{1 + (\beta\omega\tau_p)^2}{1 + (\omega\tau_p)^2}. \tag{2.18}$$

When $\rho \gg 1$ (hence, $\beta \ll 1$), (2.18) simplifies to (2.9), thus (2.18) applies to both heavy and light particles. Combining (2.18) with (2.7)–(2.11), the variance of the particle acceleration is given by

$$\left\langle \left(\frac{dv'}{dt} \right)^2 \right\rangle = \langle u'^2 \rangle \left(\frac{\beta^2}{T_L T_2} + \frac{1}{(T_L + \tau_p)(T_2 + \tau_p)} (1 - \beta^2) \right). \tag{2.19}$$

The second term on the right-hand side of (2.17) contains the acceleration variance of the fluid velocity along the particle trajectory. This is obtained by integrating over the energy spectrum (2.11):

$$\left\langle \left(\frac{Du'}{Dt} \right)^2 \right\rangle = \frac{2}{\pi} \int_0^\infty \omega^2 E(\omega) d\omega = \frac{\langle u'^2 \rangle}{T_L T_2}. \tag{2.20}$$

The final term in (2.17) contains the covariance of the particle and fluid accelerations, $\langle (dv'/dt)(Du'/Dt) \rangle$. Using the particle equation of motion (2.15), this is expressed as

$$\left\langle \frac{dv'}{dt} \frac{Du'}{Dt} \right\rangle = \tau_p^{-1} \left\langle u'_s \frac{Du'}{Dt} \right\rangle + \beta \left\langle \left(\frac{Du'}{Dt} \right)^2 \right\rangle, \tag{2.21}$$

such that

$$\langle u_s'^2 \rangle = \tau_p^2 \left\langle \left(\frac{dv'}{dt} \right)^2 \right\rangle - \tau_p^2 \beta^2 \frac{\langle u'^2 \rangle}{T_L T_2} - 2\tau_p \beta \left\langle u'_s \frac{Du'}{Dt} \right\rangle. \tag{2.22}$$

The covariance $\langle u'_s (Du'/Dt) \rangle$ can be modelled using the equilibrium Eulerian approximation proposed by Ferry & Balachandar (2001), expressed as

$$\frac{Du'}{Dt} \approx \frac{u'_s}{\tau_p(1 - \beta)}. \tag{2.23}$$

This is equivalent to setting the particle acceleration equal to the fluid acceleration in (2.15), which is tenable for small particles with $St \ll 1$ (Ferry & Balachandar 2001).

Multiplying (2.23) by the slip velocity and subsequently averaging leads to

$$\left\langle u'_s \frac{Du'}{Dt} \right\rangle = \frac{\langle u_s'^2 \rangle}{\tau_p(1-\beta)}. \quad (2.24)$$

Substituting (2.19) and (2.24) into (2.22) gives

$$\langle u_s'^2 \rangle = \langle u'^2 \rangle \frac{\tau_p^2}{(T_L + \tau_p)(T_2 + \tau_p)} (\beta - 1)^2. \quad (2.25)$$

Finally, substituting (2.16) and (2.25) into (2.3) and normalising by Kolmogorov units,

$$\begin{aligned} \frac{\langle |u_s| \rangle}{u_\eta} &= StFr^{-1} \operatorname{erf} \left\{ \left(\frac{1}{2} \frac{\langle u_s \rangle^2}{\langle u_s'^2 \rangle} \right)^{1/2} \right\} \\ &+ St \left((\beta - 1)^2 \frac{2}{\pi} \frac{\langle u'^2 \rangle}{u_\eta^2} \frac{1}{(T_L/\tau_\eta + St)(T_2/\tau_\eta + St)} \right)^{1/2} \exp \left\{ - \frac{1}{2} \frac{\langle u_s \rangle^2}{\langle u_s'^2 \rangle} \right\}, \end{aligned} \quad (2.26)$$

with

$$\frac{\langle u_s \rangle^2}{\langle u_s'^2 \rangle} = \frac{u_\eta^2}{\langle u'^2 \rangle} Fr^{-2} (\beta - 1)^{-2} (T_L/\tau_\eta + St)(T_2/\tau_\eta + St). \quad (2.27)$$

Using the above-mentioned expressions for the normalised flow velocities and timescales in terms of Re_λ , we obtain a closed-form expression for $\langle |u_s| \rangle / u_\eta$, reported in Appendix B, as a function of the governing non-dimensional parameters St , Fr , Re_λ and ρ .

The limit $\rho \ll 1$ is relevant for bubbles, which however need to remain spherical for (2.2) to be valid. This requires both the Bond number Bo and Weber number We , describing buoyancy-induced and turbulence-induced deformations, respectively, to remain below $O(1)$ (Clift *et al.* 2005; Salibindla *et al.* 2020). For air bubbles in water under terrestrial gravity, $Bo < 1$ up to diameters of 2–3 mm. The constraint $We < 1$ implies a similar limiting diameter for all but the most extreme turbulence levels, the constraints on d_p/η and St depending on the dissipation rate ε . For realistic levels up to $\varepsilon = O(1 \text{ m}^2 \text{ s}^{-3})$, the We -constraint is less restrictive than the condition $St \ll 1$ implied by invoking the equilibrium Eulerian approximation.

2.3. Marginally buoyant particles ($\rho = O(1)$)

For heavy particles, $\beta \ll 1$ such that $(\beta - 1)^2 \approx 1$ and one may use (2.26) for both $\rho \gg 1$ and $\rho \ll 1$. This approach, however, cannot be considered general as it does not apply to the case $\rho = O(1)$ or $\beta \approx 1$ (marginally buoyant particles). That is because the equilibrium Eulerian approximation we used to derive (2.26) is only valid if the particles are small. If $d_p \ll \eta$ and $\rho = O(1)$, the particles are effectively tracers, hence the slip velocity is trivially zero. The case of interest is rather the one of finite-size particles with density similar to the fluid, which have been shown to significantly lag the fluid (Homann & Bec 2010; Bellani & Variano 2012). The equilibrium Eulerian approximation is not applicable to those particles. The case of finite-size marginally buoyant particles, therefore, poses a challenge to the present framework, in that no modelling framework exists for the covariance term in (2.22). Yet, we will show that the model developed for heavy particles (which neglects unsteady forces) predicts the mean slip velocity also for such finite-size marginally buoyant particles.

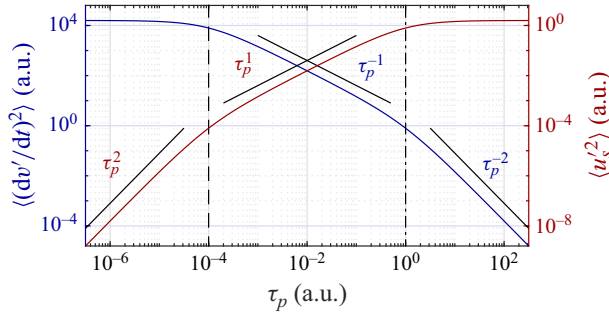


Figure 2. Trends for the acceleration variance described by the inertial filtering model (2.7)–(2.11) (left axis) and slip velocity variance given by (2.6) (right axis), both in arbitrary units. Black dashed and dash-dotted lines indicate T_2 and T_L , respectively.

3. Results and validation of the model

In the following, we illustrate the influence of these parameters in different regimes.

3.1. Heavy particles in the absence of gravity

In the absence of gravity ($Fr = \infty$) there is no mean drift, $\langle u_s \rangle = 0$, and consequently $\langle |u_s| \rangle \propto \langle u_s'^2 \rangle^{1/2}$, see (2.3) and figure 1(b). Therefore, the problem of estimating the mean slip velocity magnitude reduces to that of estimating its root-mean-square fluctuation. When $\rho \gg 1$, the slip velocity variance $\langle u_s'^2 \rangle$ is proportional to the particle acceleration variance $\langle (dv'/dt)^2 \rangle$, see (2.6). Figure 2 plots $\langle u_s'^2 \rangle$ and $\langle (dv'/dt)^2 \rangle$ as functions of τ_p in this condition, according to the analysis in § 2.1. Three distinct regimes can be identified. For particles of small inertia, $\tau_p \ll T_2$, the response function in (2.9) does not filter out a significant amount of the flow fluctuating energy; hence, the particle acceleration variance is independent of τ_p and $\langle u_s'^2 \rangle = \tau_p^2 \langle (dv'/dt)^2 \rangle \propto \tau_p^2$. In contrast, for particles of massive inertia, $\tau_p \gg T_L$, the response function modulates all relevant flow scales and the particle acceleration variance is reduced at a rate τ_p^{-2} , see (2.9); consequently, $\langle u_s'^2 \rangle$ is independent of τ_p . In the intermediate range of particle inertia, $T_2 \ll \tau_p \ll T_L$, the range of scales that is unaffected by the response function shrinks as τ_p^{-1} ; as a result, $\langle (dv'/dt)^2 \rangle \propto \tau_p^{-1}$ and $\langle u_s'^2 \rangle \propto \tau_p$.

It follows that, in the turbulence-dominated regime under study, the scaling $\langle |u_s| \rangle \propto \langle u_s'^2 \rangle^{1/2}$ in the three regimes discussed previously implies

$$\langle |u_s| \rangle / u_\eta \propto St \quad \text{for } St \ll T_2 / \tau_\eta, \tag{3.1a}$$

$$\langle |u_s| \rangle / u_\eta \propto St^{1/2} \quad \text{for } T_2 / \tau_\eta \ll St \ll T_L / \tau_\eta, \tag{3.1b}$$

$$\langle |u_s| \rangle / u_\eta = \text{constant} \quad \text{for } St \gg T_L / \tau_\eta. \tag{3.1c}$$

Equivalent relations were proposed by Balachandar (2009) based on scaling arguments, whereas here they descend from the assumptions behind the analytical model.

Figure 3(a) illustrates the modelled variation of $\langle |u_s| \rangle / u_\eta$ as a function of St for the case $Fr = \infty$, $Re_\lambda = 500$ and $\rho = 1000$, indicating the power-law scaling dependencies discussed previously. While the scaling in the intermediate regime seems unconvincing, we show in the following that this is merely a result of the limited extent of the inertial range for $Re_\lambda = 500$. In figure 3(b), $\langle |u_s| \rangle / u_\eta$ is plotted as a function of the

Model for the slip velocity of particles in turbulence

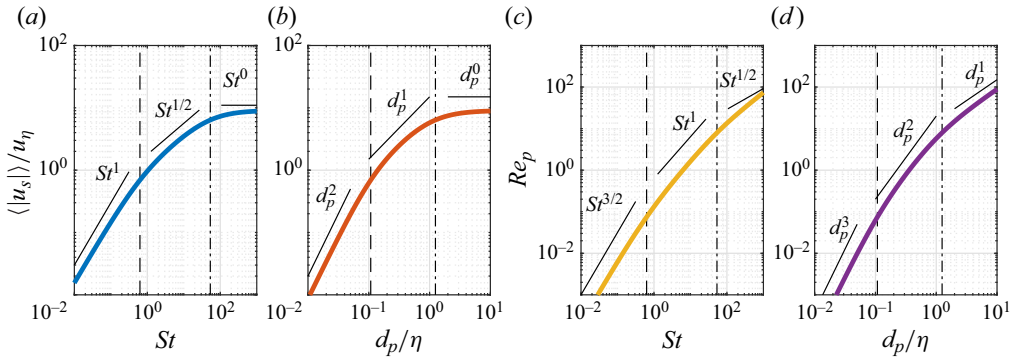


Figure 3. Variation with Stokes number modelled using (2.13) for $Re_\lambda = 500$, $Fr = \infty$ and $\rho = 1000$. Dashed and dash-dotted lines indicate T_2/τ_η and T_L/τ_η , respectively.

non-dimensional particle diameter d_p/η , whereas in figures 3(c) and 3(d), Re_p is plotted as a function of St and d_p/η , respectively. These are obtained straightforwardly from the transformations $d_p/\eta = (18St\phi(Re_p)/\rho)^{1/2}$ and $Re_p = (\langle |u_s| \rangle / u_\eta)(d_p/\eta)$, resulting in scaling dependencies highlighted in each regime (whose boundaries in terms of d_p/η depend on Re_p and ρ). To first order, in regimes where $\langle |u_s| \rangle / u_\eta \propto St^\alpha$, the changes of variables imply $\langle |u_s| \rangle / u_\eta \propto (d_p/\eta)^{2\alpha}$, $Re_p \propto St^{\alpha+1/2}$ and $Re_p \propto (d_p/\eta)^{2\alpha+1}$. When expressing Re_p as a function of St , the scaling exponent in the range $Re_p \gg 1$ deviates from $\alpha + 1/2$ due to the correction $\phi(Re_p)$.

The influence of Re_λ is illustrated in figure 4, again for $\rho = 1000$. Because $\langle u'^2 \rangle / u_\eta^2 = Re_\lambda / 15^{1/2}$, the scaling $\langle |u_s| \rangle \propto \langle u_s'^2 \rangle^{1/2}$ implies that the mean slip velocity and Re_p both increase with Re_λ . In addition, increasing Re_λ extends the inertial range and consequently the regime where $\langle |u_s| \rangle \propto St^{1/2}$ (figure 4a) and $Re_p \propto St$ (figure 4b). The scaling $\langle |u_s| \rangle \propto St^n$ is illustrated in figure 4(c), where $n = d \log \langle |u_s| \rangle / d \log St$ is plotted. This highlights the presence of a consistent scaling in the intermediate regime at high Re_λ for which a significant separation between T_2 and T_L exists.

3.2. Heavy particles in the presence of gravity

The influence of gravity on heavy particles is illustrated in figure 5, where the Froude number is reduced from $Fr = \infty$ to 0.1, keeping $Re_\lambda = 500$ and $\rho = 1000$. According to the form of the model described in § 2.1, the condition $\langle u_s \rangle^2 \gg \langle u_s'^2 \rangle$ defining the gravity-dominated regime is realised for $Fr^{-2}(T_L/\tau_\eta + St)(T_2/\tau_\eta + St) \gg 1$, see (2.14). In the limit $St \ll 1$, this corresponds to $Fr^2 \ll T_L T_2 / \tau_\eta^2$, which for the range of practical interest $Re_\lambda = O(10) - O(10^3)$ is analogous to $Fr \ll 1$. In the limit $St \gg 1$, on the other hand, the gravity-dominated regime corresponds to $Fr \ll St$. Both trends are apparent in figure 5(a): for small St , only at $Fr < 1$ can one observe significant deviations from the zero-gravity case; for large St , however, those occur for $Fr \lesssim St$. Irrespective of St , (2.13) simplifies to $\langle |u_s| \rangle / u_\eta = StFr^{-1}$ in the gravity-dominated regime, leading to the scaling $\langle |u_s| \rangle \propto St$ in figure 5(a). Similarly, figure 5(b) highlights the scaling $Re_p \propto St^2$ for $Fr \lesssim St$.

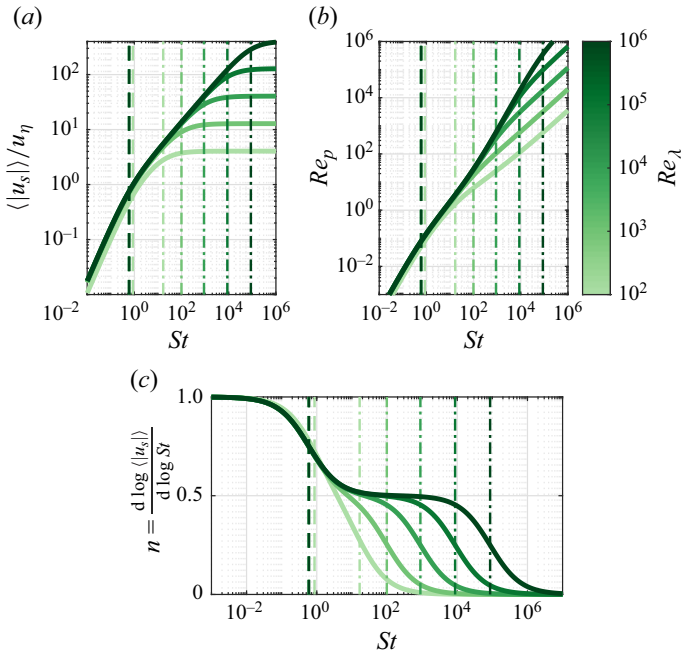


Figure 4. Influence of Re_λ on slip velocity (a) and particle Reynolds number (b), modelled using (2.13) for $Fr = \infty$ and $\rho = 1000$. Coefficient $n = d \log \langle |u_s| \rangle / d \log St$ indicating the scaling $\langle |u_s| \rangle \propto St^n$ (c). Dashed and dash-dotted lines indicate T_2/τ_η and T_L/τ_η , respectively.

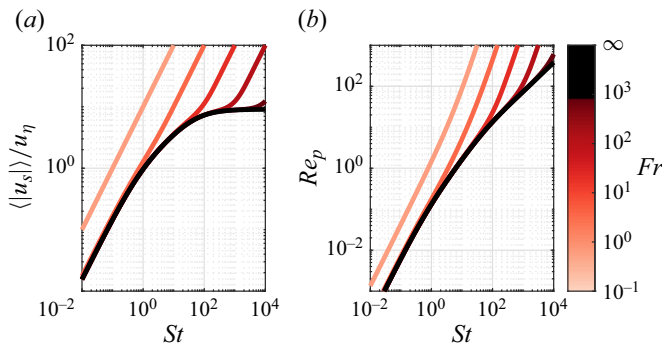


Figure 5. Influence of Fr on (a) slip velocity and (b) particle Reynolds number, modelled using (2.13) for $Re_\lambda = 500$ and $\rho = 1000$.

3.3. Influence of density ratio

The effect of density ratio ρ is demonstrated in figure 6 for $Fr = \infty$, using the analysis in §§ 2.1 and 2.2 for $\rho \gg 1$ and $\rho \ll 1$, respectively. The results for light particles are shown up to $St = 0.1$ only, following the assumption $St \ll 1$ implied by invoking the equilibrium Eulerian approximation (2.23). In such limit, the slip velocity of heavy particles in this turbulence-dominated regime scales as $\langle |u_s| \rangle \propto St$, as discussed above; while for light particles the inclusion of the unsteady forces leads to $\langle |u_s| \rangle \propto St(\beta - 1)$. Therefore, as $\beta \approx 3$ for $\rho \ll 1$, the slip velocity (and Re_p) of light particles at a given St increases as ρ decreases and can be up to a factor of two larger than for heavy particles (figure 6a,c).

Model for the slip velocity of particles in turbulence

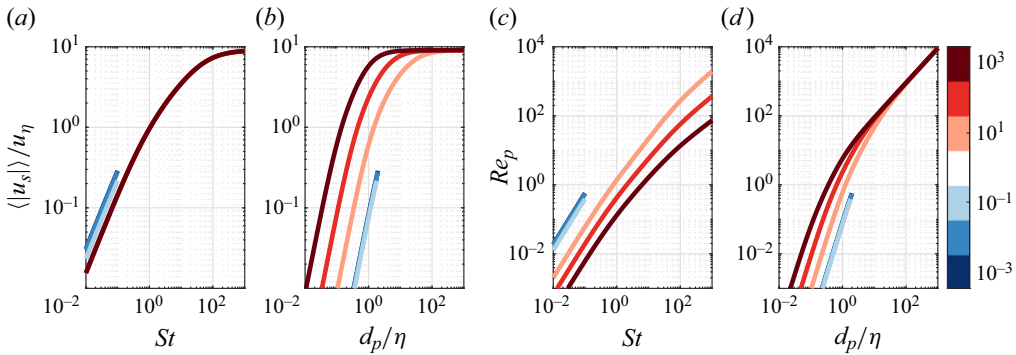


Figure 6. Influence of ρ on (a,b) slip velocity and (c,d) particle Reynolds number, modelled using (2.26) for $Re_\lambda = 500$, $Fr = \infty$.

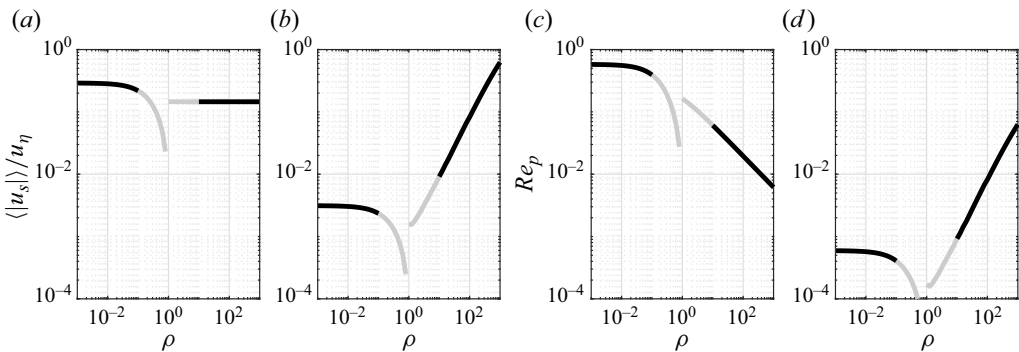


Figure 7. Influence of ρ on (a,b) slip velocity and (c,d) particle Reynolds number, modelled using (2.26) for $Re_\lambda = 500$, $Fr = \infty$ and (a,c) $St = 0.1$ or (b,d) $d_p / \eta = 0.1$.

The variations of $\langle |u_s| \rangle$ and Re_p with the particle diameter, on the other hand, follow an opposite trend: while for heavy particles $St \propto (d_p / \eta)^2 \rho$ and $\langle |u_s| \rangle \propto (d_p / \eta)^2 \rho$, for light particles $St \propto (d_p / \eta)^2 \beta^{-1}$ and $\langle |u_s| \rangle \propto (d_p / \eta)^2 (1 - \beta^{-1})$ (within finite- Re_p corrections). Therefore, at a given d_p / η , $\langle |u_s| \rangle$ and Re_p are larger for heavy particles than for light particles (figure 6b,d). The comparison between heavy and light particles in the presence of gravity leads to analogous considerations.

The effect of density ratio is isolated in figure 7, which plots the normalised slip velocity and Re_p vs ρ , fixing either $St = 0.1$ or $d_p / \eta = 0.1$ to satisfy the assumptions of the equilibrium Eulerian approximation. The black lines highlight the range $\rho < 0.1$ and $\rho > 10$ (as proxies for $\rho \ll 1$ and $\rho \gg 1$, respectively, for which the analysis in §§ 2.1 and 2.2 strictly applies). As the condition $\rho = 1$ is approached (grey lines), the model derived for light particles predicts vanishingly small slip velocities, whereas these remain finite according to the model derived for heavy particles. This observation suggests that the assumption of negligible unsteady forces may be more suitable for marginally buoyant finite-size particles, rather than including them in concert with the equilibrium Eulerian approximation. This is confirmed in the next section.

3.4. Validation

The proposed analytical model is compared against slip velocity of heavy particles, neutrally/marginally buoyant finite-size particles, and bubbles in homogeneous or

	Method	ρ	Fr	St	d_p/η	Re_λ	
Petersen <i>et al.</i> (2019)	Exp	2040	1.9	2.0–21	0.1–0.4	500	○
Clementi <i>et al.</i> (2024)	Exp	7.8	0.001–0.01	0.08–0.4	0.7–1.4	234–445	□
Bellani & Variano (2012)	Exp	1	∞	12	21	115	◇
Uhlmann & Chouippe (2017)	Num	1.5	∞	2.5–11	5.5–11	117–142	◊
Cisse <i>et al.</i> (2013)	Num	1	∞	10–73	17–67	160	△
Ma <i>et al.</i> (2020)	Num	0.001	0.02	0.5	12	17	○
Zhang <i>et al.</i> (2019)	Num	0.001	∞	0.02–2	0.7–7	216	□

Table 1. Experimental and numerical studies reporting mean slip velocity of particles in homogeneous turbulence. Petersen, Baker & Coletti (2019), Bellani & Variano (2012) and Clementi, Wedi & Coletti (2024) used facing random jet arrays to generate homogeneous turbulence. Cisse, Homann & Bec (2013) and Uhlmann & Chouippe (2017) carried out particle-resolved simulations with an immersed boundary method in forced homogeneous isotropic turbulence, whereas Zhang *et al.* (2019) followed a point-particle approach. Ma *et al.* (2020) considered the centre-plane region in a vertical channel flow simulated by the immersed boundary method.

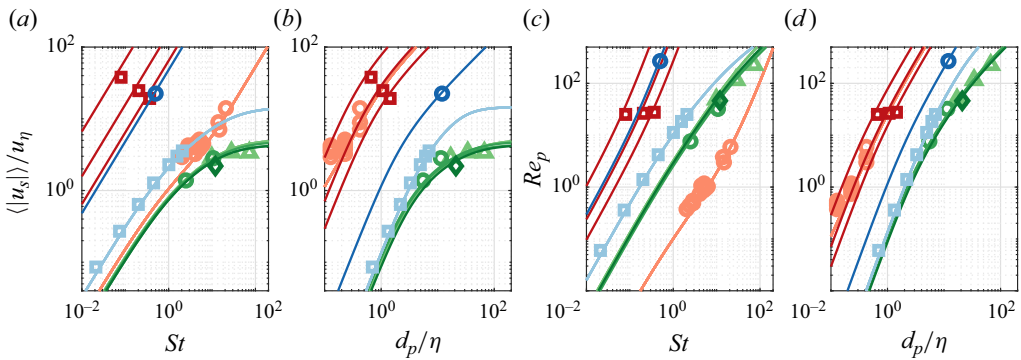


Figure 8. Validation of model of particle slip velocity in homogeneous turbulence. The various cases from numerical and experimental data are summarised in table 1. Symbols represent reported values; lines of the same colour represent model predictions. For comparison with Ma *et al.* (2020), only the *SmFew* case is considered as the model is limited to the one-way coupled regime.

quasi-homogeneous turbulence, as observed in laboratory experiments and direct numerical simulations listed in table 1. This allows us to validate the analysis across all practically interesting regions of the parameter space. For marginally buoyant finite-size particles, we deploy the form of the model derived in § 2.1 which neglects unsteady forces. The estimate of the fluid velocity at the particle location is discussed in the referenced works and extensively in other experimental and numerical studies (e.g. Horwitz & Mani 2016; Berk & Coletti 2021). The specific approaches may lead to different instantaneous values, but the average of the observable is not expected to differ significantly. As shown in figure 8, the model is in quantitative agreement with the data for all regimes.

4. Conclusions

Building on the framework of inertial filtering, we have developed an analytical model which captures the slip velocity magnitude of spherical non-tracer particles in homogeneous turbulence over the wide parameter space spanned by practically relevant applications, from light to heavy particles, from microscopic to finite size. The model takes

two forms, derived for particles heavier and lighter than the fluid. The former retains only drag force and gravity effects, and is shown to be applicable also to marginally buoyant finite-size particles. The latter includes added mass and stress gradient forces and leverages the equilibrium Eulerian approximation, which in turn assumes small and weakly inertial particles.

The model is in quantitative agreement with experiments and direct numerical simulations. This has three important implications. First, it demonstrates that, for the purpose of predicting the magnitude of the mean slip velocity, the assumptions made are tenable. Those include: (i) Gaussian distribution of the slip velocity; (ii) small impact of history force and lift force, both neglected in the model; (iii) validity of the equilibrium Eulerian approximation for small light particles; (iv) negligible importance of unsteady forces for marginally buoyant particles; and (v) negligible difference between the flow scales experienced by particles and tracers. The prediction of higher-order observables, such as higher-order moments and two-point statistics, may require some of those simplifications to be relaxed. Second, the model is proven to yield valuable physical insight, capturing the specific influence of individual parameters on the slip velocity. Isolating the effect of each parameter is crucial for the predictive understanding of particle-laden turbulence, but is virtually impossible in physical experiments and typically beyond the reach of numerical simulations. Third, the ample validation warrants that the proposed model can make accurate predictions of the mean slip velocity purely from the governing parameters of the system. Therefore, we expect it to be useful for studies in which the slip velocity is an important parameter, e.g. to determine whether the dispersed phase is an accurate tracer and whether it is likely to back-react on the carrier fluid.

The model provides a theoretical underpinning for empirical observations which hitherto have only been qualitatively explained. For example, neutrally buoyant particles reportedly behave as tracers as long as $d_p/\eta \lesssim 5$ (Qureshi *et al.* 2007; Volk *et al.* 2011). Figure 8 shows how, for Re_λ typical of experimental and numerical studies, this is precisely the size limit beyond which the mean slip velocity is not negligible, $\langle |u_s| \rangle > u_\eta$. In this regard, our results are complementary to those of Mathai *et al.* (2016) who predict how particle accelerations depart from those of tracers as function of St/Fr . The present model also makes new predictions yet to be verified, specifically at high Re_λ .

Several extensions of the present model are possible. For example, the observed intermittency in the slip velocity distribution can be incorporated, which may be important to predict higher-order moments. The history force can be included if an integral expression is used, such as that proposed in Ling *et al.* (2013) which however is only valid in a limited portion of the parameter space. Similarly, the lift force may be added using scaling dependencies with the governing parameters (Saffman 1956; Rubinow & Keller 1961). Moreover, the model could be extended to non-homogeneous turbulence, using expressions for the temporal and velocity scale ratios valid for, e.g., turbulent boundary layers. Finally, the present framework may be applied to the important case of non-spherical particles (Voth & Soldati 2017), provided that the equation of motion is adequately parametrised.

Acknowledgements. The authors are grateful to T. Ma, M. Clementi and M. Wedi for providing their respective datasets.

Funding. The present work was supported in part by the US Army Research Office, Division of Earth Materials and Processes (grant W911NF-17-1-0366) and Division of Fluid Dynamics (grant W911NF-18-1-0354), and in part by the Swiss National Science Foundation (grant number 200021-207318).

Declaration of interests. The authors report no conflict of interest.

Author ORCID*s*.

Tim Berk <https://orcid.org/0000-0002-7159-2360>;

Filippo Coletti <https://orcid.org/0000-0001-5344-2476>.

Appendix A

Using the relations provided at the end of § 2.1, the heavy-particle model given by (2.13) and (2.14) can be expressed in closed form as

$$\begin{aligned} \frac{\langle |u_s| \rangle}{u_\eta} &= StFr^{-1} \operatorname{erf} \left\{ \left(\frac{1}{2} \frac{\langle u_s \rangle^2}{\langle u_s'^2 \rangle} \right)^{1/2} \right\} \\ &+ St \left(\frac{2}{\pi} \frac{Re_\lambda}{15^{1/2}} \right)^{1/2} \left(\frac{Re_\lambda + 32}{135^{1/2}(1 - (0.1Re_\lambda)^{-1/2})} + St \right)^{-1/2} \\ &\times \left(\frac{6(1 - (0.1Re_\lambda)^{-1/2})}{10(1 + 110Re_\lambda^{-1})^{-1}} + St \right)^{-1/2} \exp \left\{ - \frac{1}{2} \frac{\langle u_s \rangle^2}{\langle u_s'^2 \rangle} \right\}, \end{aligned} \tag{A1}$$

with

$$\begin{aligned} \frac{\langle u_s \rangle^2}{\langle u_s'^2 \rangle} &= \frac{15^{1/2}}{Re_\lambda} Fr^{-2} \left(\frac{Re_\lambda + 32}{135^{1/2}(1 - (0.1Re_\lambda)^{-1/2})} + St \right) \\ &\times \left(\frac{6(1 - (0.1Re_\lambda)^{-1/2})}{10(1 + 110Re_\lambda^{-1})^{-1}} + St \right). \end{aligned} \tag{A2}$$

Appendix B

Using the relations provided at the end of 2.1, the light-particle model given by (2.26) and (2.27) can be expressed in closed form as

$$\begin{aligned} \frac{\langle |u_s| \rangle}{u_\eta} &= StFr^{-1} \operatorname{erf} \left\{ \left(\frac{1}{2} \frac{\langle u_s \rangle^2}{\langle u_s'^2 \rangle} \right)^{1/2} \right\} \\ &+ St(\beta - 1) \left(\frac{2}{\pi} \frac{Re_\lambda}{15^{1/2}} \right)^{1/2} \left(\frac{Re_\lambda + 32}{135^{1/2}(1 - (0.1Re_\lambda)^{-1/2})} + St \right)^{-1/2} \\ &\times \left(\frac{6(1 - (0.1Re_\lambda)^{-1/2})}{10(1 + 110Re_\lambda^{-1})^{-1}} + St \right)^{-1/2} \exp \left\{ - \frac{1}{2} \frac{\langle u_s \rangle^2}{\langle u_s'^2 \rangle} \right\}, \end{aligned} \tag{B1}$$

with

$$\begin{aligned} \frac{\langle u_s \rangle^2}{\langle u_s'^2 \rangle} &= \frac{15^{1/2}}{Re_\lambda} Fr^{-2} (\beta - 1)^{-2} \left(\frac{Re_\lambda + 32}{135^{1/2}(1 - (0.1Re_\lambda)^{-1/2})} + St \right) \\ &\times \left(\frac{6(1 - (0.1Re_\lambda)^{-1/2})}{10(1 + 110Re_\lambda^{-1})^{-1}} + St \right). \end{aligned} \tag{B2}$$

REFERENCES

- BALACHANDAR, S. 2009 A scaling analysis for point-particle approaches to turbulent multiphase flows. *Intl J. Multiphase Flow* **35** (9), 801–810.
- BALACHANDAR, S. & EATON, J.K. 2010 Turbulent dispersed multiphase flow. *Annu. Rev. Fluid Mech.* **42** (1), 111–133.
- BALACHANDAR, S., PENG, C. & WANG, L.P. 2024 Turbulence modulation by suspended finite-sized particles: toward physics-based multiphase subgrid modeling. *Phys. Rev. Fluids* **9** (4), 044304.
- BEC, J., GUSTAVSSON, K. & MEHLIG, B. 2024 Statistical models for the dynamics of heavy particles in turbulence. *Annu. Rev. Fluid Mech.* **56** (1), 189–213.
- BELLANI, G. & VARIANO, E.A. 2012 Slip velocity of large neutrally buoyant particles in turbulent flows. *New J. Phys.* **14** (12), 125009.
- BERK, T. & COLETTI, F. 2021 Dynamics of small heavy particles in homogeneous turbulence: a Lagrangian experimental study. *J. Fluid Mech.* **917**, A47.
- BRANDT, L. & COLETTI, F. 2022 Particle-laden turbulence: progress and perspectives. *Annu. Rev. Fluid Mech.* **54** (1), 159–189.
- CISSE, M., HOMANN, H. & BEC, J. 2013 Slipping motion of large neutrally buoyant particles in turbulence. *J. Fluid Mech.* **735**, R1.
- CLEMENTI, M., WEDI, M. & COLETTI, F. 2024 Reduced settling of heavy particles in homogeneous turbulence. In *1st European Fluid Dynamics Conference*, 16–20 September 2024, Aachen, Germany.
- CLIFT, R., GRACE, J. & WEBER, M.E. 2005 *Bubbles, Drops and Particles*. Dover.
- CSANADY, G.T. 1963 Turbulent diffusion of heavy particles in the atmosphere. *J. Atmos. Sci.* **20** (3), 201–208.
- DAITCHE, A. 2015 On the role of the history force for inertial particles in turbulence. *J. Fluid Mech.* **782**, 567–593.
- FERRY, J. & BALACHANDAR, S. 2001 A fast Eulerian method for disperse two-phase flow. *Intl J. Multiphase Flow* **27** (7), 1199–1226.
- GATIGNOL, R. 1983 The Faxen formulae for a rigid particle in an unsteady non-uniform Stokes flow. *J. Mec. Theor. Appl.* **2** (2), 143–60.
- HALLER, G. 2019 Solving the inertial particle equation with memory. *J. Fluid Mech.* **874**, 1–4.
- HINZE, J.O. 1975 *Turbulence*. Mcgraw-Hill.
- HOMANN, H. & BEC, J. 2010 Finite-size effects in the dynamics of neutrally buoyant particles in turbulent flow. *J. Fluid Mech.* **651**, 81–91.
- HORWITZ, J.A.K. & MANI, A. 2016 Accurate calculation of Stokes drag for point-particle tracking in two-way coupled flows. *J. Comput. Phys.* **318**, 85–109.
- LIEN, R.-C. & D'ASARO, E.A. 2002 The Kolmogorov constant for the Lagrangian velocity spectrum and structure function. *Phys. Fluids* **14** (12), 4456–4459.
- LING, Y., PARMAR, M. & BALACHANDAR, S. 2013 A scaling analysis of added-mass and history forces and their coupling in dispersed multiphase flows. *Intl J. Multiphase Flow* **57**, 102–114.
- MA, T., LUCAS, D., JAKIRLIĆ, S. & FRÖHLICH, J. 2020 Progress in the second-moment closure for bubbly flow based on direct numerical simulation data. *J. Fluid Mech.* **883**, A9.
- MATHAI, V., CALZAVARINI, E., BRONS, J., SUN, C. & LOHSE, D. 2016 Microbubbles and microparticles are not faithful tracers of turbulent acceleration. *Phys. Rev. Lett.* **117** (2), 024501.
- MATHAI, V., LOHSE, D. & SUN, C. 2020 Bubbly and buoyant particle-laden turbulent flows. *Annu. Rev. Condens. Matter Phys.* **11** (1), 529–559.
- MAXEY, M. 2017 Simulation methods for particulate flows and concentrated suspensions. *Annu. Rev. Fluid Mech.* **49** (1), 171–193.
- MAXEY, M.R. & RILEY, J.J. 1983 Equation of motion for a small rigid sphere in a nonuniform flow. *Phys. Fluids* **26** (4), 883–889.
- MORDANT, N., LÉVÊQUE, E. & PINTON, J.-F. 2004 Experimental and numerical study of the Lagrangian dynamics of high Reynolds turbulence. *New J. Phys.* **6** (1), 116.
- OKA, S. & GOTO, S. 2022 Attenuation of turbulence in a periodic cube by finite-size spherical solid particles. *J. Fluid Mech.* **949**, A45.
- OLIVIERI, S., PICANO, F., SARDINA, G., IUDICONE, D. & BRANDT, L. 2014 The effect of the basset history force on particle clustering in homogeneous and isotropic turbulence. *Phys. Fluids* **26** (4), 041704.
- OUELLETTE, N.T., XU, H., BOURGOIN, M. & BODENSCHATZ, E. 2006 Small-scale anisotropy in Lagrangian turbulence. *New J. Phys.* **8** (6), 102.
- PARMAR, M., ANNAMALAI, S., BALACHANDAR, S. & PROSPERETTI, A. 2018 Differential formulation of the viscous history force on a particle for efficient and accurate computation. *J. Fluid Mech.* **844**, 970–993.
- PETERSEN, A.J., BAKER, L. & COLETTI, F. 2019 Experimental study of inertial particles clustering and settling in homogeneous turbulence. *J. Fluid Mech.* **864**, 925–970.

- POZORSKI, J. & MINIER, J.-P. 1998 On the Lagrangian turbulent dispersion models based on the Langevin equation. *Intl J. Multiphase Flow* **24** (6), 913–945.
- PRASATH, S.G., VASAN, V. & GOVINDARAJAN, R. 2019 Accurate solution method for the Maxey–Riley equation, and the effects of Basset history. *J. Fluid Mech.* **868**, 428–460.
- PUMIR, A. & WILKINSON, M. 2016 Collisional aggregation due to turbulence. *Annu. Rev. Condens. Matter Phys.* **7** (1), 141–170.
- QURESHI, N.M., BOURGOIN, M., BAUDET, C., CARTELLIER, A. & GAGNE, Y. 2007 Turbulent transport of material particles: an experimental study of finite size effects. *Phys. Rev. Lett.* **99** (18), 184502.
- RUBINOW, S.I. & KELLER, J.B. 1961 The transverse force on a spinning sphere moving in a viscous fluid. *J. Fluid Mech.* **11** (3), 447–459.
- SAFFMAN, P.G. 1956 On the motion of small spheroidal particles in a viscous liquid. *J. Fluid Mech.* **1** (5), 540–553.
- SALIBINDLA, A.K.R., MASUK, A.U.M., TAN, S. & NI, R. 2020 Lift and drag coefficients of deformable bubbles in intense turbulence determined from bubble rise velocity. *J. Fluid Mech.* **894**, A20.
- SAWFORD, B.L. 1991 Reynolds number effects in Lagrangian stochastic models of turbulent dispersion. *Phys. Fluids A* **3** (6), 1577–1586.
- SAWFORD, B.L., YEUNG, P.K., BORGAS, M.S., VEDULA, P., LA PORTA, A., CRAWFORD, A.M. & BODENSCHATZ, E. 2003 Conditional and unconditional acceleration statistics in turbulence. *Phys. Fluids* **15** (11), 3478–13489.
- TENNETI, S. & SUBRAMANIAM, S. 2014 Particle-resolved direct numerical simulation for gas–solid flow model development. *Annu. Rev. Fluid Mech.* **46** (1), 199–230.
- UHLMANN, M. & CHOUPIPE, A. 2017 Clustering and preferential concentration of finite-size particles in forced homogeneous-isotropic turbulence. *J. Fluid Mech.* **812**, 991–1023.
- VOLK, R., CALZAVARINI, E., LÉVÊQUE, E. & PINTON, J.-F. 2011 Dynamics of inertial particles in a turbulent von Kármán flow. *J. Fluid Mech.* **668**, 223–235.
- VOTH, G.A. & SOLDATI, A. 2017 Anisotropic particles in turbulence. *Annu. Rev. Fluid Mech.* **49** (1), 249–276.
- ZAICHIK, L.I., SIMONIN, O. & ALIPCHENKOV, V.M. 2003 Two statistical models for predicting collision rates of inertial particles in homogeneous isotropic turbulence. *Phys. Fluids* **15** (10), 2995–3005.
- ZHANG, Z., LEGENDRE, D. & ZAMANSKY, R. 2019 Model for the dynamics of micro-bubbles in high-Reynolds-number flows. *J. Fluid Mech.* **879**, 554–578.